

Article

Magnetic and Optical Properties of Natural Diamonds with Subcritical Radiation Damage Induced by Fast Neutrons

Nikolai A. Poklonski ¹, Andrey A. Khomich ², Ivan A. Svito ¹, Sergey A. Vyrko ¹, Olga N. Poklonskaya ¹, Alexander I. Kovalev ¹, Maria V. Kozlova ^{2,3}, Roman A. Khmel'nitskii ^{2,4} and Alexander V. Khomich ^{2,4,*}

¹ Faculty of Physics, Belarusian State University, Nezavisimosti Ave. 4, 220030 Minsk, Belarus; poklonski@bsu.by (N.A.P.); svito@bsu.by (I.A.S.); olga.poklonskaya@tut.by (O.N.P.)

² Kotelnikov Radio-Engineering and Electronics Institute of the Russian Academy of Sciences, Vvedensky sq. 1, 141190 Fryazino, Russia; antares-610@yandex.ru (A.A.K.); marija-kozlova@yandex.ru (M.V.K.); khmel'nitskya@lebedev.ru (R.A.K.)

³ Faculty of Physics, Lomonosov Moscow State University, Leninskie Gory 1, bld. 1, 119991 Moscow, Russia

⁴ Lebedev Physical Institute of the Russian Academy of Sciences, Leninsky av. 53, 119991 Moscow, Russia

* Correspondence: alex-khomich@mail.ru

Abstract: Raman spectroscopy and magnetic properties of the natural single crystalline diamonds irradiated with high fluences of fast reactor neutrons have been investigated. Raman spectra transformations were studied in the range from moderate levels up to radiation damage leading to diamond graphitization. The selection of fast neutrons irradiated diamonds for magnetic measurements was carried out according to Raman scattering data on the basis of the intensity criterion and the spectral position of the “1640” band. It was found that in natural diamonds irradiated with neutrons with an extremely high subcritical fluence $F = 5 \times 10^{20} \text{ cm}^{-2}$, the transition from a diamagnetic to a ferromagnetic state is observed at the Curie–Weiss temperature of $\approx 150 \text{ K}$. The energy of the exchange magnetic interaction of uncompensated spins is estimated to be $\approx 1.7 \text{ meV}$. The differential magnetic susceptibility estimated from the measurements of magnetic moment for temperature 2 K in the limit of $B \approx 0$ is $\chi_{\text{diff}} \approx 1.8 \times 10^{-3} \text{ SI units}$. The nature of magnetism in radiation-disordered single-crystal hydrogen- and metal-free natural diamond grains was discussed.

Keywords: diamond; neutron irradiation; nanostructured materials; magnetics; Raman spectra



Citation: Poklonski, N.A.; Khomich, A.A.; Svito, I.A.; Vyrko, S.A.; Poklonskaya, O.N.; Kovalev, A.I.; Kozlova, M.V.; Khmel'nitskii, R.A.; Khomich, A.V. Magnetic and Optical Properties of Natural Diamonds with Subcritical Radiation Damage Induced by Fast Neutrons. *Appl. Sci.* **2023**, *13*, 6221. <https://doi.org/10.3390/app13106221>

Academic Editors: Elena Korznikova and Andrey Kistanov

Received: 30 March 2023

Revised: 15 May 2023

Accepted: 17 May 2023

Published: 19 May 2023



Copyright: © 2023 by the authors. Licensee MDPI, Basel, Switzerland. This article is an open access article distributed under the terms and conditions of the Creative Commons Attribution (CC BY) license (<https://creativecommons.org/licenses/by/4.0/>).

1. Introduction

Inducing intrinsic magnetism in the nominally nonmagnetic carbon materials containing only s- and p-electrons is an intriguing yet challenging task [1]. The experimental discovery of magnetism in polymerized fullerenes [2] and in graphite irradiated with protons [3,4] has stimulated numerous experimental and theoretical studies of the magnetic properties of pure carbon structures. Lightweight non-metallic magnetic carbon materials with a Curie point above room temperature are very promising for applications in medicine and biology as a unique biocompatible magnet [5] as well as in nanotechnology, telecommunications, and carbon electronics.

The variety of chemical compounds of carbon is explained by the ability of its s- and p-electrons to form hybrid electronic orbitals in different proportions. The electronic subsystem of a cooperative system of carbon atoms is very labile and is characterized by many metastable states, while transitions from one state to another are possible (switching effects) even with the same fixed configuration of nuclei. The allotropy of carbon leads to the formation of pure carbon structures with a wide variety of and often opposite properties [6]. Therefore, it is not surprising that the main experimental successes towards obtaining pure carbon ferromagnets are associated with films or 2D objects with close proportions of sp^3 and sp^2 carbon, and high concentration of defects, including hydrogenated ones, in which

hydrogen seems to play a stabilizing role, preventing the transition of sp^3 carbon to sp^2 carbon. Various synthesis methods have been tried to obtain magnetic carbon.

The defect-induced magnetism in carbon materials (mainly ion-implanted diamonds) was studied experimentally and theoretically in [7–14] etc. Two mutually consistent basic models dominated for a long time, explaining the manifestations of the magnetism of pure carbon materials—the “amorphous” one with variable sp^3/sp^2 -carbon hybridization [15] and the “hydrogen” one, according to which the decisive role of reactive hydrogen was assumed [16].

The measurements [17] confirmed the ferromagnetism of proton-irradiated carbon films without metal impurities. The superparamagnetism found [18] during measurements on a SQUID magnetometer in proton-irradiated diamonds grown in high-pressure autoclaves (HPHT synthesis) was explained by the interaction of amorphous carbon (formed upon irradiation) and ferromagnetic impurities contained in the HPHT sample. Unusual behavior of the magnetic moment in HPHT synthetic nitrogen-doped diamond crystals was also observed due to the existence of superparamagnetic and superconducting regions [19]. Measurements on a SQUID magnetometer in [20] irradiated with 1–2 MeV proton beams ultra-pure CVD (chemically vapor deposited) diamonds confirmed the presence of high-temperature paramagnetic properties. Based on photoluminescence data, it was suggested that vacancies have a decisive influence on magnetism in diamonds. However, the Raman spectra presented in the same article [20] do not support this hypothesis.

CVD diamond crystals implanted with deuterium ions [21] also demonstrate magnetism. A hysteresis was observed in the CW-ESR (continuous wave electron spin resonance) spectra of CVD diamonds implanted with hydrogen isotopes and annealed in vacuum at temperatures in the range from 1000 to 1300 °C, which indicates the ordering of electron spins. This effect was enhanced in natural diamonds implanted with hydrogen in the channeling mode. The absence of ferromagnetic impurities in the untreated crystals of natural and CVD diamond and the coincidence of C–H bond breaking temperatures and disappearance of hysteresis in EPR spectra made it possible to consider deuterium (hydrogen)–vacancy complexes as the most probable cause of spin ordering. Ferromagnetism was revealed [22] in nanocrystalline diamond films implanted with 35 keV nitrogen. It should be noted that nanocrystalline CVD diamond films usually contain up to 1–2 at.% of hydrogen located at intercrystallite boundaries, which may be a piece of evidence in favor of the “hydrogen” model of magnetism in irradiation-modified diamonds. In the case of pure diamond, Talapatra et al. [23] reported the existence of ferromagnetic hysteresis at room temperature in the magnetization of nanograins of diamond after nitrogen and carbon irradiation.

Ferromagnetism with a Curie temperature of about 500 K was discovered in ultrathin layers of so-called Q-carbon with a predominantly amorphous structure [24–26], which is formed during the melting and rapid cooling of a carbon film after exposure to nanosecond laser pulses. The fraction of sp^3 carbon in Q-carbon is from 75 to 85%, and the remaining carbon atoms are sp^2 hybridized [24].

Ferromagnetism in a carbon film deposited in a radio frequency discharge was confirmed by measurements on a SQUID magnetometer [27] and explained by changes in the sp^2/sp^3 carbon ratio. Carbon microspheres with a diameter of about 3 μm containing graphitized nanocrystals with a thickness of 5–15 layers of graphene were obtained by pyrolysis, which exhibits ferromagnetic properties [28].

Magnetic ordering was observed in graphite and graphene oxide as a result of implantation with 100 MeV gold ions [29], as well as upon implantation of highly oriented pyrolytic graphite (HOPG) separately with carbon and hydrogen ions [30]. It is reported [31] on the production of pyrolytic magnetic carbon with the concentration of uncompensated electron spins of $(3.5 \pm 0.7) \times 10^{15}$ spins/mg. Magnetic ordering at room temperature was also obtained for polyaniline composites containing carbon quantum dots [32].

Due to high processability, studies of the magnetic properties of laser-graphitized films are of special interest. The observation of a stable ferromagnetic response at a temperature

of 300 K from a 20 nm thick surface layer formed in the cut region of diamond crystal by a laser (wavelength 532 nm, energy 0.5 mJ, pulse duration 200 ns at the frequency of 15 kHz) is reported [33]. In this case, the magnetic moment measured by the SQUID magnetometer was observed only for crystals that were cut by a laser along the (100) surface orientation. The magnetic signals were much weaker for (110) and negligible for (111) laser-cut diamond surfaces. The dependence of the structure of the laser-graphitized layer on the crystallographic orientation of the diamond surface was previously discovered in [34,35]. The ferromagnetic signal (coercive fields ≈ 8 mT) disappeared after chemical etching or after moderate temperature annealing. According to [33], the results indicate that laser processing of diamond can lead to the creation of ferromagnetic spots on its surface. This phenomenon can be of interest not only for memory devices but also for other rather subtle applications [36–39], such as using a localized magnetic spot near a nitrogen–carbon vacancy (NV-center) to influence its magneto-optical response, especially to increase its field sensitivity at certain applied field ranges. The processability of this approach arises from the ability of laser radiation to locally form NV centers in the volume of diamond samples [38–40].

Current understanding about the mechanisms of ferromagnetism of pure carbon materials is actively developing. Various causes capable of inducing a magnetic state in pure carbon systems have been considered: defects in the crystal lattice [8,12], band ferromagnetism [41], and negatively curved sp^2 -bonded nanoregions in carbon structures [42], vacancy-hydrogen complexes [43], hydrogen passivated vacancies in graphene [44], etc. To explain ferromagnetism in graphite irradiated with high-energy protons, models based on the formation of networks of point defects due to grain boundaries [45] or high concentrations of vacancies [46] were proposed in [3]. As for the magnetic properties of Q-carbon and amorphous carbon, a model was proposed in [15] that makes it possible to explain the magnetic properties of these materials by the presence of unpaired electrons in three-coordinated sp^2 -carbon atoms. In a later publication [47], the assumption was substantiated that in amorphous carbon and Q-carbon having a low specific density, carbon chains, i.e., sp^1 and sp^2 carbon, are responsible for magnetism. Thus, despite significant efforts, there is currently no generally accepted point of view and understanding of the nature of magnetism in pure carbon materials. Moreover, it is not clear whether the mechanism of formation of the magnetic state is common for all carbon systems or whether it differs for different allotropes.

The formation of a magnetic state in sp^2 -carbon materials can be considered an established experimental fact, but these materials, unlike diamonds, do not have outstanding physical and chemical properties. Diamond is considered a promising material for high-temperature electronics and spintronics. Weak spin-orbit and hyperfine interactions in diamond contribute to a large diffusion length and coherence time of the electron spin and thus create the necessary conditions for spin manipulation. Irradiation of diamonds with fast reactor neutrons, which modify uniformly their bulk properties in a wide range of damage [48,49], is one of the ways to form a magnetic state in diamonds. In [50], metastable spin states (of a spin glass type) were found at room temperature in the absence of illumination by CW-ESR measurements in CVD diamond films irradiated with fast reactor neutrons.

It should be noted that in a number of studies, false positive results may have been obtained, since metal mills were used to prepare samples of carbon materials, which, in combination with the exceptional hardness of diamond, led to contamination of the samples with metals. False positive results can also be obtained from measurements of diamond crystals. The ambiguity of the results of magnetic measurements for diamonds is often due to studies of synthetic crystals that may contain processing impurities of d- and f-elements. A paramagnetic or ferromagnetic contribution in nominally non-magnetic materials also may originate from magnetic impurities present in the carbon materials. These are diamond grown in HPHT synthesis, in which catalyst metals (Fe, Ni, and Co) are used to dissolve graphite. Besides, additional special measures should be taken in the experimental study of magnetic properties [51]. Polycrystalline CVD diamond films deposited in an activated

plasma (usually a mixture of methane and hydrogen) can contain high concentrations of chemically bound hydrogen, localized mainly at intercrystallite boundaries, as well as paramagnetic nitrogen in substitution positions, which makes it difficult to establish the nature of magnetism in diamond between “amorphous” and “hydrogen” models.

The purpose of this work is to study the effect of fast neutron irradiation with high but subcritical fluences (which does not lead to irreversible graphitization) on the magnetic state of single-crystal hydrogen- and metal-free natural diamond grains.

2. Materials and Methods

To study the magnetic properties, single-crystal natural diamond grains of IIa type with an average “diameter” of ≈ 0.5 mm, irradiated with fast reactor neutrons with fluences close to the critical damage level of diamond, were selected according to their Raman data. At the critical level of radiation damage, diamonds are irreversibly transformed into a graphite-like material during subsequent high-temperature annealing. Diamonds irradiated with fast neutrons are better suited for studying the radiation-induced transformations of the crystal structure than diamonds after ion implantation. The interaction cross-section of neutrons with carbon atoms is small; therefore, the radiation damage due to these interactions is uniformly distributed over the whole crystal volume. As reference samples, we used natural and CVD diamonds, both irradiated with fast neutrons and implanted with helium ions.

Irradiation with fast neutrons was carried out in the nuclear reactor of the National Research Center “Kurchatov Institute” [52] and in the IVV-2M research nuclear reactor of the Institute of Metal Physics of Ural Branch of Russian Academy of Sciences [48], while implantation with helium ions was performed at the “High Voltage Engineering Europa B.V.” ion accelerator. Raman spectra were measured under laboratory conditions on Horiba Jobin Yvon Lab-RAM HR (Lille, France) and Nanofinder HE (Lotis TII-Tokyo Instruments, Tokyo, Japan) spectrometers with excitation at 473 and 532 nm, respectively. The resolution of these Raman spectrometers was $\Delta\nu_R = 0.5\text{--}1.0\text{ cm}^{-1}$. The samples were annealed in an oven with graphite walls, in a vacuum of 10^{-5} Torr, at temperatures from 200 to 1700 °C (for 60 min at fixed temperature). After the heat treatment, the samples were etched in a hot $\text{H}_2\text{SO}_4 + \text{K}_2\text{Cr}_2\text{O}_7$ solution at ≈ 180 °C, to remove graphite that might be formed on external surfaces. Cleaning of the virgin and irradiated grains of natural diamond (113 pcs of each type, average grain diameter of ≈ 0.5 mm) from possible magnetic contamination on the surface was carried out by etching in hot acids, as well as in a quartz test tube (successively filled with alcohol and distilled water) placed in an ultrasonic bath PSB-1335-05 “Ecoton” filled with water. The ultrasound frequency was 35 kHz, and the power of the ultrasound generator was 50 W. The processing time of virgin and irradiated diamond grains in each liquid under laboratory conditions was 10 min. Recommendations [51,53] were taken into account to exclude possible sources of magnetic contamination of diamond grains.

Magnetic measurements in the range of magnetic field B from -8 to 8 T were carried out on a High Field Cryogen Free Measurement System with a Vibrating Sample Magnetometer (Cryogenic Ltd., London, UK) in the temperature range from 2 to 300 K. The magnetic field B was swept at a rate of up to 0.1 T/min. The samples were placed in a thin-walled hard gelatin ampoule and sealed with dry cotton to fix their position during the measurements. The ampoule with samples was fixed in a thin-walled polypropylene tube mounted at the end of the vibration head rod. The rod vibration frequency was 21 Hz. The oscillation amplitude was in the range of 1–2 mm.

3. Results and Discussion

3.1. Raman Spectra of Neutron-Irradiated Diamonds

Raman scattering is an informative nondestructive method for the analysis of a wide class of carbon materials. Figure 1 shows the Raman spectra of irradiation-modified natural and CVD diamonds. In the unirradiated diamond, the maximum of Raman line was at 1332.4 cm^{-1} , and FWHM (full width at half maximum) is $\approx 2\text{ cm}^{-1}$. The irradiation with

fast neutrons with fluence $F = 3 \times 10^{18} \text{ cm}^{-2}$ leads to a decrease in the intensity of diamond Raman peak, an increase in FWHM up to $\approx 6 \text{ cm}^{-1}$, and a shift of the diamond line to 1328.8 cm^{-1} . The maximum of the band near 1630 cm^{-1} , which is characteristic of the Raman spectra of radiation damaged diamonds [54,55], was at 1634 cm^{-1} . The spectra also contain a rather sharp defect-induced band at 1420 cm^{-1} , which is attributed to intrinsic defect containing interstitial atoms [56].

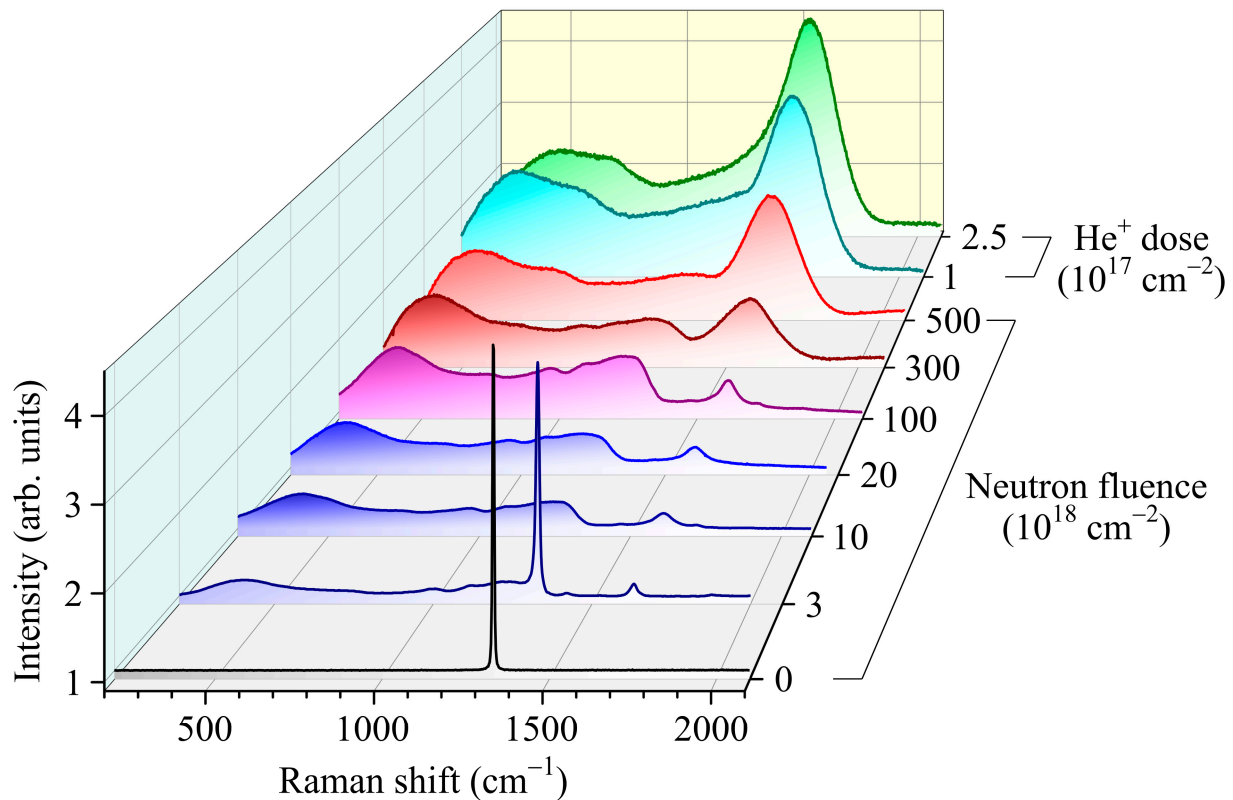


Figure 1. Raman spectra of natural and CVD diamonds unirradiated and irradiated with fast reactor neutrons with fluences F from 3×10^{18} to $5 \times 10^{20} \text{ cm}^{-2}$ (see also [49]) or uniformly implanted with multiple-energy keV helium ions with a total dose of 1×10^{17} and $2.5 \times 10^{17} \text{ cm}^{-2}$. All spectra were recorded with excitation at wavelength $\lambda = 473 \text{ nm}$ except for the spectra at $F = 3 \times 10^{18} \text{ cm}^{-2}$, which was recorded with excitation at $\lambda = 532 \text{ nm}$.

In the low-frequency region of the spectrum of diamond irradiated with fast neutrons with fluence $F = 3 \times 10^{18} \text{ cm}^{-2}$, a wide structural band dominates with singularities $990, 1008, 1120,$ and 1235 cm^{-1} , which exactly coincide with phonon frequencies at the singular points of the Brillouin zone $LA(L), LA(K)$ and $TO(W), TO(K), LO(K),$ and $LO(L)$, respectively [56–58]. In the range of $900\text{--}1300 \text{ cm}^{-1}$, the spectrum is close to the spectrum of the phonon density of states (PDOS) of diamond [59]. The appearance of these singularities in the Raman spectra is attributed to phonon confinement effect [60,61] due to the high concentration of intrinsic irradiation-induced defects and consequently a decrease in the phonon mean free path L_{ph} in radiation damaged diamond [49]. The broad low-frequency band with a maximum at about 400 cm^{-1} (Figure 1) coincides with the band observed in natural diamonds implanted with helium ions [54,62], as well as in nanodiamonds [61,63]. Historically, such a peak in disordered materials has been called the boson peak [64,65]. According to our studies [62], amorphous diamond is unstable under normal conditions and due to the pressure from the diamond matrix can exist only in the form of nano-inclusions. The coexistence of amorphous and crystalline regions in radiation-damaged diamond is also noticeable in the Raman spectra, in which there is simultaneously a diamond peak, a

wide band with a spectrum close to PDOS of diamond, as well as a boson peak characteristic of amorphous diamond.

A further increase in the neutron fluence (up to $1 \times 10^{19} \text{ cm}^{-2}$ and higher) leads to broadening, weakening, and low-frequency shift of the diamond peak in the Raman spectra (Figure 1), which is typical for radiation-disordered diamonds [41,54,66–68] with the phonon mean free path $L_{\text{ph}} < 5 \text{ nm}$ [49]. The absence of a diamond peak in the Raman spectra is partly explained by the fact that the cross section for Raman scattering of light in diamond is much smaller than in other allotropic forms of carbon. As the fluence (level of radiation damage) increases, the maximum of the boson peak shifts slightly towards higher frequencies, and its relative intensity increases, which indicates an increase in the volume fraction of amorphized diamond in the samples. At the same time, the intensity of a broad band of unidentified nature with a maximum near 720 cm^{-1} increases (Figure 1). It is possible that the band at 720 cm^{-1} is associated with a feature of the vibrational density of states activated by the disorder of the sp^2 phase [69]. The position, relative amplitude, and FWHM of the band around $1600\text{--}1640 \text{ cm}^{-1}$ are most sensitive to the neutron fluence (Figure 1). As the neutron fluence increases from 3×10^{18} to $5 \times 10^{20} \text{ cm}^{-2}$, the relative intensity of this band increases significantly, and its maximum shifts to low frequencies up to 1574 cm^{-1} (Figures 1 and 2).

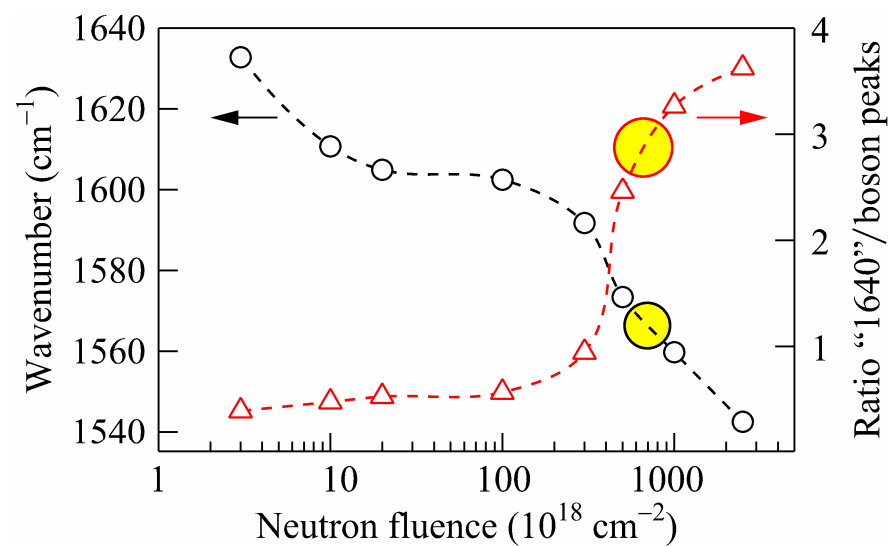


Figure 2. Position (left axis) of the “1640” band and ratio “1640”-to-boson peaks (right axis) in Raman spectra of natural diamonds irradiated with fast neutrons or He-implanted as functions of radiation damage. Dashed lines are guides to eyes. Yellow circles show the position of the “1640” band and ratio “1640”-to-boson peaks corresponding to the critical level of radiation damage of diamond.

The position of the “1640” band is higher than the graphitic mode at 1580 cm^{-1} (G peak) [70], which is doubly degenerate (TO and LO) phonon mode (E_{2g} symmetry) at the center of the Brillouin zone. The nature of the “1640” band in diamonds with a damage level below the critical level is complex. The measurements were performed on ion-implanted and fast neutron-irradiated diamonds [55], and the “1640” band consists of several peaks, which shift to higher frequencies and become narrower with decreasing in the radiation damage level. The decomposition of the “1640” band showed that it consists of at least six Gaussian peaks (FWHM of $6\text{--}10 \text{ cm}^{-1}$), which shift to lower frequencies and become wider with increasing in the radiation damage level [55]. These peaks appear to refer to various irradiation-induced defects. The observed sharpness of the peaks indicates that they originate from well-defined local rather than extended defects. As the level of radiation damage increases, the concentration of defects of this type and tensile stresses increase, and their structure can change, which leads to a low-frequency shift and broadening of the corresponding bands in the Raman spectra (Figures 1 and 2).

Multiple-energy implantation of helium ions makes it possible to receive the uniform distribution of radiation defects in ion-implanted areas in diamonds, including those with a level above the critical level [62] (two upper spectra in Figure 1). Radiation damage to diamonds above the critical level abruptly changes the mechanical and physicochemical properties of diamond [62], while the Raman spectra change almost monotonously. The features associated with phonon confinement in diamond disappear in them [13], and the maximum of the most intense band shifts from 1574 cm^{-1} (at $F = 5 \times 10^{20}\text{ cm}^{-2}$) to 1567 and 1542 cm^{-1} in the spectra of natural diamonds implanted with helium ions with a total dose of 1×10^{17} and $2.5 \times 10^{17}\text{ cm}^{-2}$, respectively [62]. Radiation damage of diamonds during multiple-energy helium implantation [62] with total dose of $1 \times 10^{17}\text{ cm}^{-2}$ approximately corresponds to the degree of disorder achieved when they are irradiated with fast neutrons [52] with fluence of $1 \times 10^{21}\text{ cm}^{-2}$. Thus, the intensity and position of the maximum of the “1640” band can serve as an indicator of the degree of radiation damage to the diamond. The selection for magnetic measurements of natural diamond grains irradiated with fast neutrons was carried out according to Raman scattering data on the basis of the intensity criterion and the spectral position of the “1640” band (see Figure 2), i.e., having the highest subcritical level of radiation damage. Rapid changes near the critical level of radiation damage of diamond in the spectral position of the “1640” band and the intensity of this band in comparison with the boson band (Figure 2) demonstrate the advantage of this technique over establishing the level of diamond critical damage based on the calculated value of vacancies [71] as deduced from the TRIM [72] computer code, the magnitude of mechanical stresses in the ion-implanted layer [73], or by the value of crystal lattice expansion [74]. The necessity of selecting diamonds for magnetic measurements is conditioned by different levels of radiation damage of diamond grains simultaneously irradiated in the fast reactor neutron flux (due to local variations of heat dissipation conditions).

One of the goals of this work was to develop an algorithm for quantitative determination of the level of radiation damage of diamond. As a measure of radiation damage in ion implantation, the calculations of vacancy concentration using the SRIM computer algorithm are often used, which is based on the statistical Monte Carlo method, the pair collision approximation, and the semiempirical description of the potentials of the interaction of fast particles with electronic and atomic subsystems [75]. SRIM modeling correctly describes the distribution profiles of implanted impurity and radiation defects and gives in many respects a good agreement with experiment, but it has a number of limitations. Modeling according to SRIM algorithm does not take into account the crystalline nature of the bombarded substance (in particular, channeling), does not consider the interaction between defects and their diffusion, that is, it gives a “frozen” picture of primary point defects, and does not consider phenomena during the accumulation of radiation damage, including the so-called “ballistic annealing”, when, at high implantation doses under conditions of a high concentration of defects, collision with an already knocked-out atom does not lead to the formation of a new defect and can even return the atom to the substituting position [76]. The concentrations of point defects calculated using SRIM should be used with great care at high levels of radiation damage, since under such conditions, the calculated concentration of vacancies can exceed the concentration of carbon atoms in diamond. In addition, SRIM modeling cannot predict the structure of the damaged material and its change during relaxation and annealing.

The second problem in calculating the level of radiation damage is the irradiation conditions themselves: the temperature of irradiation and the content of impurities, primarily nitrogen [77].

A change in the microstructure of a material during radiation damage leads to its swelling due to a decrease in density. This phenomenon is observed in all materials, but in diamond, it is most pronounced and is accompanied by an increase in the crystal lattice parameter, determined by X-ray [74] and neutron [48] diffraction. Strong (up to 40 vol.%) swelling in radiation-damaged diamond is one of the evidences in favor of the hypothesis of the formation of an amorphous material with density of $\approx 2\text{ g/cm}^3$ [71,77,78] and poorly

manifested in X-ray diffraction. The value of swelling varies nonmonotonically during subsequent annealings [77], which in some cases does not allow the use of swelling as a quantitative measure of radiation damage. In the case of natural diamond crystallites with irregular geometric shapes, the comparison of sample sizes before and after irradiation is rather problematic.

In this paper, to determine the degree of radiation damage, including critical damage, it is proposed to use Raman spectra. Figure 2 shows changes in the position of the maximum of the intense band “1640” in neutron-irradiated (with subcritical level of radiation damage) and ion-implanted (with the level of radiation damage above critical, annealing at 1400 °C led to continuous graphitization of ion-implanted layers) natural diamonds. When comparing the level of radiation damage of neutron-irradiated diamonds and helium-implanted, it was taken into account that diamonds with a total helium dose of $0.5 \times 10^{17} \text{ cm}^{-2}$ recovered their crystal structure during high-temperature annealing.

As can be seen in Figure 2, the position of maximum of “1640” band and the ratio of its amplitude to the amplitude of the boson peak can serve as good indicators of exceeding the critical level of radiation damage to diamond. It is important to note that both parameters in Figure 2 in the Raman spectra of diamonds implanted with helium ions at doses of 1.0×10^{17} and $2.5 \times 10^{17} \text{ cm}^{-2}$ practically did not change during the subsequent annealing at temperatures at least to 500 °C until graphitization processes (appearance of the D band in the Raman spectra) of diamond implanted with helium ions with dose of $2.5 \times 10^{17} \text{ cm}^{-2}$ began. This indicates the possibility of using the dependences in Figure 2 for the non-destructive determination of the critical damage of diamonds in the case of their moderate heating during irradiation.

The transformations of the Raman spectra during successive annealings (1 h at each temperature) were studied in order to confirm that the level of diamond radiation damage remains below the critical level under irradiation with fast neutrons with fluence of $5 \times 10^{20} \text{ cm}^{-2}$ (Figure 3). As the annealing temperature rises, the diamond peak is restored, and the bands are narrowed and shifted towards higher frequencies.

The transformations of the “1640” band are of particular interest. This band has an asymmetric shape; after annealing at temperatures above 800 °C, several separate bands are spectrally resolved in it (as was observed in [55] in the Raman spectra of diamonds with a lower level of radiation damage), decreasing to the background level after annealing at temperatures above 1000 °C (Figure 3).

The intensity of the two-phonon Raman band ($2800\text{--}3500 \text{ cm}^{-1}$) also significantly decreases after annealing at temperatures above 1000 °C (Figures 3 and 4). The spectral shape of the two-phonon Raman band for neutron-irradiated diamonds differs significantly both from the same spectrum for undamaged diamond with a maximum near 2335 cm^{-1} [56], and from the spectra for a wide class of sp^2 -carbon materials, which dominate the band with a maximum near 2685 cm^{-1} [79]. For example, the Raman spectrum of HOPG, treated graphite that displays the highest degree of three-dimensional ordering, consists of two main bands observed at 1581 and 2687 cm^{-1} , denoted as the G band and 2D (or G') band, respectively [80,81]. The 2D band corresponds to the second-order Raman scattering of an in-plane transverse optical (TO) mode close to the Brillouin zone boundary K point [82].

Decomposition of the “1640” band into Lorentz contours (Figure 4) showed that it consists of at least three components with maxima near 1465 , 1530 , and 1620 cm^{-1} , and the four main components of the second-order band are presumably overtones of the “1640” band components with frequencies approximately equal to twice the first-order frequencies (2925 , 3050 and 3230 cm^{-1} , respectively) and a combination of the $1530 + 1620 \text{ cm}^{-1}$ ($\approx 3135 \text{ cm}^{-1}$) components. In this case, it should be kept in mind that the lattice parameter of neutron-irradiated crystals is increased compared to unirradiated diamond [48,74], which causes a shift of the bands in the Raman spectra to the low-frequency region [49,54,55,67].

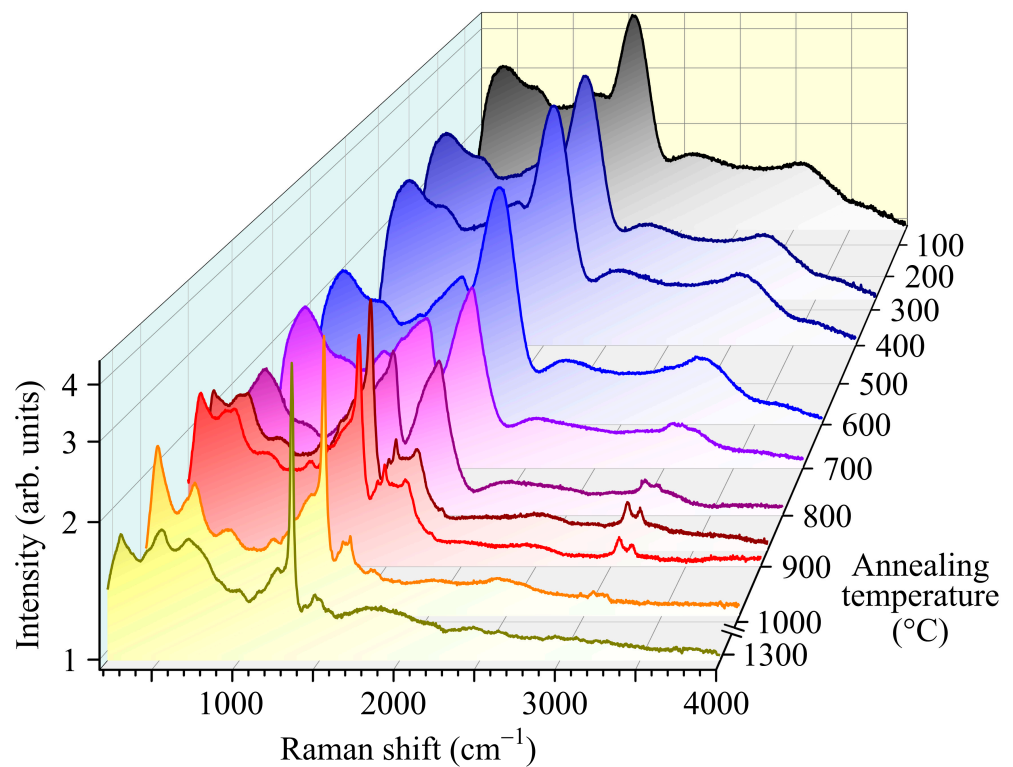


Figure 3. Transformation of the Raman spectra of fast neutron-irradiated natural diamond crystal with fluence of $5 \times 10^{20} \text{ cm}^{-2}$ depending on the annealing temperature (1 h at each temperature in the range of 100–1300 °C = 373–1573 K). Spectra were recorded with excitation at $\lambda = 473 \text{ nm}$.

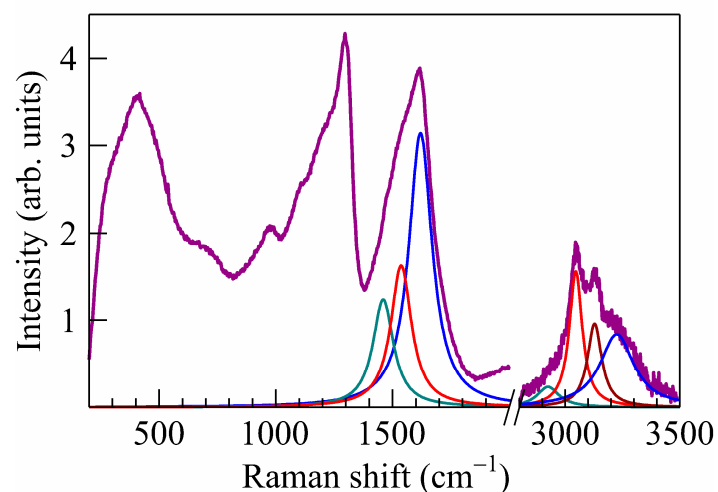


Figure 4. Deconvolution of “1640” and second-order bands of the Raman spectra of fast neutron-irradiated ($F = 5 \times 10^{20} \text{ cm}^{-2}$) natural diamond after its annealing at 800 °C (see Figure 3). The contours of the Lorentzian form of the “1640” band of the first and second order are shown in color.

Thus, the data of Raman spectroscopy indicate that the level of radiation damage in natural diamonds irradiated with fast neutrons ($F = 5 \times 10^{20} \text{ cm}^{-2}$) is below the critical value. At the same time, the samples studied here contain inside amorphous diamond inclusions and are materials with mixed sp^2/sp^3 hybridization of carbon without the formation of bulk inclusions of the sp^2 phase. This is in good agreement with the neutron-diffraction measurements of CVD diamond irradiated with fast neutrons with $F = 3 \times 10^{20}$ and $5 \times 10^{20} \text{ cm}^{-2}$ [48]. The absence of impurities of d- and f-elements, as well as chemically bound hydrogen, in the bulk of the samples, makes them a good

model material for studying the magnetic properties of pure carbon materials with the diamond structure.

3.2. Magnetic Properties of Diamonds Irradiated with Fast Neutrons

Figure 5 shows the results of measurements of the magnetic moment M of natural diamond grains irradiated with fast neutrons and selected by Raman spectroscopy (113 pcs, average grain diameter of ≈ 0.5 mm) as a function of magnetic field B in the temperature range from 2 to 300 K. Virgin (unirradiated) diamond grains (also 113 pcs, average grain diameter of ≈ 0.5 mm) were diamagnetic in the temperature range from 2 to 300 K with the magnetic susceptibility $\chi_{\text{diff}} \approx -1 \times 10^{-5}$ SI units. According to quantum chemical calculations [83], the magnetic susceptibility of unirradiated natural diamond (in SI units [84,85]) is equal $\chi_{\text{SI}} = 4\pi\chi_{\text{cgs}} = -(1.9\text{--}2.1) \times 10^{-5}$. Handbook [86] gives the value of the specific magnetic susceptibility of natural diamond for $T = 100\text{--}293$ K as $\chi_{\rho} = -6.2 \times 10^{-6}$ cm³/g; considering the density of unirradiated diamond grains $\rho_{\text{vir}} = 3.515$ g/cm³ [87], we have (in SI units) $\chi = \rho_{\text{vir}}\chi_{\rho} = -2.2 \times 10^{-5}$.

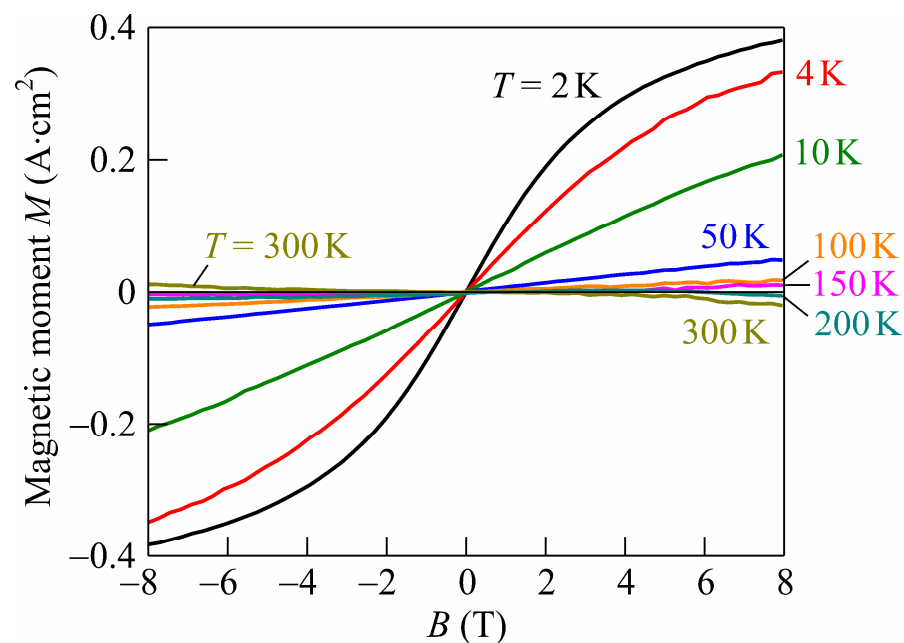


Figure 5. Magnetic moment M of natural diamond grains (113 pcs) irradiated with fast reactor neutrons ($F = 5 \times 10^{20}$ cm⁻²). The measurement absolute temperatures (T from 2 to 300 K) are shown in the figure.

Note that, in the virgin (not irradiated with neutrons) grains of natural diamond, the CW-ESR signal was not observed at room temperature [88]. It was shown there that irradiation of natural diamond grains with neutrons (with fluence $F \approx 1 \times 10^{21}$ cm⁻² above critical level of radiation damage) led to the appearance of an intense CW-ESR signal from metastable paramagnetic centers with paramagnetic relaxation times $>10^{-5}$ s. The possible reason for this signal appearance in irradiated diamond is the metastable non-compensated spins located on the inner surface of nanopores (clusters of vacancies in diamond crystal matrix).

According to [89], the energy of the exchange interaction of uncompensated spins is $J = 2k_{\text{B}}\Theta/z$, where k_{B} is the Boltzmann constant. For the number of geometric neighbors in a random system $z \approx 15.47$ [90] and the Curie–Weiss temperature $\Theta = 150$ K (at which the magnetic moment of irradiated diamond is zero; see Figure 5), we have $J \approx 1.7$ meV. Note that the observed Curie–Weiss temperature Θ is close to the temperature of ≈ 145 K, observed for carbon nanofoam (see Figure 3 in [13]).

Figure 6 shows the dependences of the differential magnetic susceptibility χ_{diff} on B (calculated from the data in Figure 5 using the formula $\chi_{\text{diff}}(B) = (\mu_0/V)dM/dB$, where $\mu_0 = 1.25 \mu\text{H/m}$ is the magnetic constant) for the volume $V \approx 7.4 \text{ mm}^3$ of 113 diamond grains irradiated with fast neutrons. It can be seen that the differential magnetic susceptibility of irradiated diamond grains at the temperature of 2 K in the limit of zero external magnetic field ($B \approx 0$) is $\chi_{\text{diff}}(B \approx 0) \approx 1.8 \times 10^{-3}$ SI units.

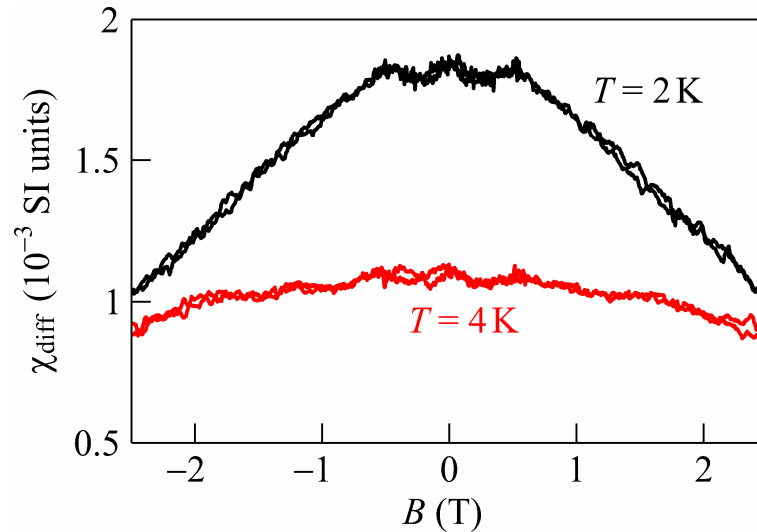


Figure 6. Differential magnetic susceptibility $\chi_{\text{diff}}(B) = (\mu_0/V)dM/dB$ (in SI units) of natural diamond grains (113 pcs, $V \approx 7.4 \text{ mm}^3$) irradiated with fast neutrons ($F = 5 \times 10^{20} \text{ cm}^{-2}$). The measurement absolute temperatures ($T = 2$ and 4 K) are shown in the figure.

This value almost coincides with the experiment [48], where the SQUID measurements of neutron irradiated polycrystalline CVD diamond films without metallic impurities for $F = 5 \times 10^{20} \text{ cm}^{-2}$ at the temperature $T = 2 \text{ K}$ show $\chi \approx 1.7 \times 10^{-3}$ SI units. CVD polycrystalline diamonds are grown on foreign substrates (typically silicon) with a microwave plasma CVD system using methane–hydrogen mixtures. Such films contained rather high concentration ($\sim 10^{20} \text{ cm}^{-3}$) of bounded hydrogen (CH_x groups) located at the intercrystalline boundaries. It was shown earlier [91] that neutrons act on grain boundaries in diamond dislodging hydrogen into the grain bulk for distances of the order of a few micrometers. At the same time, numerous defects are formed, including those with uncompensated spin. The presence of high concentrations of hydrogen-containing defects explained the manifestations of magnetism in various carbon materials [4,16,18,21,22]. The coincidence of the values of the magnetic susceptibility measured in this work for natural hydrogen-free diamonds and in the [48] for CVD diamond films irradiated with fast neutrons with the same fluence ($5 \times 10^{20} \text{ cm}^{-2}$) indicates that hydrogen-containing radiation defects do not significantly affect the magnetic properties of radiation-disordered diamonds.

In Figure 6, a nonmonotonic dependence of χ_{diff} on B is seen in the range from -0.5 to 0.5 T for $T = 2 \text{ K}$, which may be due to the heating and cooling of diamond grains during their magnetization reversal. This finds support in measurements [92,93], where the thermal nature of the nonmonotonicity of hopping magnetoresistance in semiconductor materials (Ge of p -type and 3C-SiC of n -type) at temperatures below 1.5 K is shown. Note that irradiation of IIa diamond grains with neutron fluence of $3 \times 10^{20} \text{ cm}^{-2}$ led to a noticeable increase in dielectric losses with maximum at frequency of 50 kHz [94].

Recently, many new artificial ferromagnetic materials have been discovered and investigated, which were made by introducing defects into nonmagnetic host crystals [95,96]. Diamond as a pure carbon material with its high material purity is a good candidate for the investigation of defect-induced ferromagnetism after graphitic materials [3,7,29,43–45], silicon carbide [96], and oxides [97].

The nature of the defects responsible for magnetism in radiation-modified diamonds remains questionable. The data presented above testify in favor of the fact that the magnetism in the samples under study is due to intrinsic defects of radiation origin. In diamonds with a moderated level of damage, we previously detected [98] the so-called amber centers [99,100], which are large spherical aggregates consisting of 40 to 60 vacancies [101]. However, at high levels of damage, the conditions for diffusion of vacancies change significantly, and the absorption bands characteristic of amber centers with maxima near 4100 cm^{-1} are not observed in the IR spectra. We believe that the most probable defects providing ferromagnetism in diamond are centers with variable sp^2/sp^3 hybridization. As is known, the maximum phonon frequency in a pure sp^3 carbon material does not exceed 1350 cm^{-1} . The centers that appear in the Raman spectra in the composition of the “1640” band contain single or chain C=C groups. This feature cannot be assigned to any pure form of sp^3 -carbon [102]. Judging by the Raman spectra, the concentration of centers that appear in the $1400\text{--}1800\text{ cm}^{-1}$ range is quite high. The behavior of a system of dilute defects in a host lattice that interact magnetically on a finite lengthscale can be described using percolation theory [103]. Such studies are in progress.

4. Conclusions

The magnetic properties of hydrogen-free natural diamond samples with the highest possible degree of radiation disordering (or subcritical radiation damage) were studied. The selection of irradiated with fast neutron diamonds was carried out according to their Raman spectra. It was found that Raman spectra of diamonds with extremely high subcritical radiation damage have an intense band with a maximum near 1575 cm^{-1} , boson peak, and a structural band at $900\text{--}1300\text{ cm}^{-1}$ due to the phonon confinement effect. It is shown that in the diamonds with subcritical radiation damage, the Raman band with a maximum near 1575 cm^{-1} is a superposition of at least three bands with maxima at 1465 , 1530 and 1620 cm^{-1} , and the overtones of these three bands and a combination band $1530 + 1620\text{ cm}^{-1}$ dominate in the second-order Raman spectra of such samples. It is shown that both the position of the maximum of the intense band near 1575 cm^{-1} and the ratio of the amplitudes of this band and the boson peak with a maximum near 420 cm^{-1} can serve as a criterion for reaching the level of critical radiation damage of diamond. The magnetic moment of natural diamond grains irradiated with fast neutrons was measured at cryogenic temperatures. For the first time, it has been established that for the observed Curie–Weiss temperature $\Theta \approx 150\text{ K}$ of the transition from the ferromagnetic to the diamagnetic state, the energy of the exchange magnetic interaction of uncompensated spins is $J \approx 1.7\text{ meV}$. The differential magnetic susceptibility of irradiated diamond grains with subcritical radiation damage (113 pcs, with a total volume $V \approx 7.4\text{ mm}^3$) at the temperature of 2 K in the limit of zero external magnetic field ($B \approx 0$) is $\chi_{\text{diff}}(B \approx 0) \approx 1.8 \times 10^{-3}$ SI units. Virgin diamond grains of the same quantity and total volume in the temperature range from 2 to 300 K were diamagnetic with $\chi_{\text{diff}} \approx -1 \times 10^{-5}$ SI units.

The most probable defects that provide ferromagnetism in diamond are the centers with variable sp^2/sp^3 hybridization, which are observed in Raman spectra in the spectral range $1400\text{--}1800\text{ cm}^{-1}$ characteristic for sp^2/sp^3 hybridization, namely, in the intense Raman band with a maximum near 1575 cm^{-1} . The coincidence of the magnetic susceptibility values measured in this work for natural hydrogen-free diamonds and the literature data for CVD diamond films irradiated with fast neutrons with almost the same fluence ($5 \times 10^{20}\text{ cm}^{-2}$) indicates that hydrogen-containing radiation defects do not have a significant effect on the magnetic properties of radiation-disordered diamonds.

Author Contributions: Conceptualization, N.A.P., A.V.K. and A.A.K.; methodology N.A.P. and A.V.K.; validation, S.A.V. and A.V.K.; investigation, N.A.P., A.V.K., A.A.K., I.A.S., O.N.P., A.I.K., M.V.K. and R.A.K.; writing—original draft preparation, A.V.K.; writing—review and editing, N.A.P. and A.A.K.; visualization, S.A.V. and A.A.K.; project administration, N.A.P. and A.A.K.; funding acquisition, N.A.P. and A.A.K. All authors have read and agreed to the published version of the manuscript.

Funding: The reported study was funded by Russian Science Foundation, grant no. 22-72-10108 “Fundamental studies of structure transformations, optical and magnetic properties of diamond under the influence of fast neutron irradiation, ion implantation and femtosecond laser radiation” (Raman study), Belarusian National Research Program “Materials Science, New Materials and Technologies” and by Belarusian Republican Foundation for Fundamental Research, grant No. F21RM-137.

Data Availability Statement: Additional data is available upon request to the corresponding authors.

Acknowledgments: A.A.K. and M.V.K. acknowledge the financial support from the Russian Science Foundation; N.A.P. and S.A.V. acknowledge the financial support from the Belarusian National Research Program “Materials Science, New Materials and Technologies”; A.I.K. acknowledges the financial support from the Belarusian Republican Foundation for Fundamental Research (grant No. F21RM-137); R.A.K. and A.V.K. thanks for the financial support provided within the framework of state task from the Ministry of Science and Higher Education of the Russian Federation to the Kotelnikov Institute of Radio Engineering and Electronics of Russian Academy of Sciences.

Conflicts of Interest: The authors declare no conflict of interest.

References

1. Ivanovskii, A.L. Magnetic effects induced by sp impurities and defects in nonmagnetic sp materials. *Phys.-Usp.* **2007**, *50*, 1031–1052. [[CrossRef](#)]
2. Makarova, T.L.; Sundqvist, B.; Höhne, R.; Esquinazi, P.; Kopelevich, Y.; Scharff, P.; Davydov, V.A.; Kashevarova, L.S.; Rakhmanina, A.V. Magnetic carbon. *Nature* **2001**, *413*, 716–718. [[CrossRef](#)] [[PubMed](#)]
3. Esquinazi, P.; Setzer, A.; Höhne, R.; Semmelhack, C.; Kopelevich, Y.; Spemann, D.; Butz, T.; Kohlstrunk, B.; Lösche, M. Ferromagnetism in oriented graphite samples. *Phys. Rev. B* **2002**, *66*, 024429. [[CrossRef](#)]
4. Esquinazi, P.; Spemann, D.; Höhne, R.; Setzer, A.; Han, K.-H.; Butz, T. Induced Magnetic Ordering by Proton Irradiation in Graphite. *Phys. Rev. Lett.* **2003**, *91*, 227201. [[CrossRef](#)] [[PubMed](#)]
5. Bennet, K.E.; Tomshine, J.R.; Min, H.-K.; Manciu, F.S.; Marsh, M.P.; Paek, S.B.; Settell, M.L.; Nicolai, E.N.; Blaha, C.D.; Kouzani, A.Z.; et al. A Diamond-Based Electrode for Detection of Neurochemicals in the Human Brain. *Front. Hum. Neurosci.* **2016**, *10*, 102. [[CrossRef](#)]
6. Poklonski, N.A.; Vyrko, S.A.; Siahlo, A.I.; Poklonskaya, O.N.; Ratkevich, S.V.; Hieu, N.N.; Kocherzhenko, A.A. Synergy of physical properties of low-dimensional carbon-based systems for nanoscale device design. *Mater. Res. Express* **2019**, *6*, 042002. [[CrossRef](#)]
7. Fujita, M.; Wakabayashi, K.; Nakada, K.; Kusakabe, K. Peculiar Localized State at Zigzag Graphite Edge. *J. Phys. Soc. Jpn.* **1996**, *65*, 1920–1923. [[CrossRef](#)]
8. Shibayama, Y.; Sato, H.; Enoki, T.; Endo, M. Disordered Magnetism at the Metal-Insulator Threshold in Nano-Graphite-Based Carbon Materials. *Phys. Rev. Lett.* **2000**, *84*, 1744–1747. [[CrossRef](#)]
9. Nakada, K.; Fujita, M.; Dresselhaus, G.; Dresselhaus, M.S. Edge state in graphene ribbons: Nanometer size effect and edge shape dependence. *Phys. Rev. B* **1996**, *54*, 17954–17961. [[CrossRef](#)]
10. Andriotis, A.N.; Menon, M.; Sheetz, R.M.; Chernozatonskii, L. Magnetic Properties of C₆₀ Polymers. *Phys. Rev. Lett.* **2003**, *90*, 026801. [[CrossRef](#)]
11. Kusakabe, K.; Maruyama, M. Magnetic nanographite. *Phys. Rev. B* **2003**, *67*, 092406. [[CrossRef](#)]
12. Kim, Y.-H.; Choi, J.; Chang, K.J.; Tománek, D. Defective fullerenes and nanotubes as molecular magnets: An ab initio study. *Phys. Rev. B* **2003**, *68*, 125420. [[CrossRef](#)]
13. Rode, A.V.; Gamaly, E.G.; Christy, A.; Fitz Gerald, J.G.; Hyde, S.; Elliman, R.; Luther-Davies, B.; Veinger, A.I.; Androulakis, J.; Giapintzakis, J. Unconventional magnetism in all-carbon nanofoam. *Phys. Rev. B* **2004**, *70*, 054407. [[CrossRef](#)]
14. Höhne, R.; Esquinazi, P.; Heera, V.; Weishart, H. Magnetic properties of ion-implanted diamond. *Diam. Relat. Mater.* **2007**, *16*, 1589–1596. [[CrossRef](#)]
15. Sakai, Y.; Chelikowsky, J.R.; Cohen, M.L. Magnetism in amorphous carbon. *Phys. Rev. Mater.* **2018**, *2*, 074403. [[CrossRef](#)]
16. Esquinazi, P.; Höhne, R.; Han, K.-H.; Setzer, A.; Spemann, D.; Butz, T. Magnetic carbon: Explicit evidence of ferromagnetism induced by proton irradiation. *Carbon* **2004**, *42*, 1213–1218. [[CrossRef](#)]
17. Ohldag, H.; Tyliszczak, T.; Höhne, R.; Spemann, D.; Esquinazi, P.; Ungureanu, M.; Butz, T. π -Electron Ferromagnetism in Metal-Free Carbon Probed by Soft X-Ray Dichroism. *Phys. Rev. Lett.* **2007**, *98*, 187204. [[CrossRef](#)]
18. Daya, N.; Sideras-Haddad, E.; Makgato, T.N.; García-Hernández, M.; Climent-Font, A.; Zucchiatti, A.; Ramos, M.A. Investigation of the magnetic properties of proton irradiated type Ib HPHT diamond. *Diam. Relat. Mater.* **2016**, *64*, 197–201. [[CrossRef](#)]
19. Barzola-Quiquia, J.; Stiller, M.; Esquinazi, P.D.; Molle, A.; Wunderlich, R.; Pezzagna, S.; Meijer, J.; Kossack, W.; Buga, S. Unconventional Magnetization below 25 K in Nitrogen-doped Diamond provides hints for the existence of Superconductivity and Superparamagnetism. *Sci. Rep.* **2019**, *9*, 8743. [[CrossRef](#)]
20. Makgato, T.; Sideras-Haddad, E.; Ramos, M.; García-Hernández, M.; Climent-Font, A.; Zucchiatti, A.; Muñoz-Martin, A.; Shrivastava, S.; Erasmus, R. Magnetic properties of point defects in proton irradiated diamond. *J. Magn. Magn. Mater.* **2016**, *413*, 76–80. [[CrossRef](#)]

21. Khomich, A.V.; Khmel'nitskiy, R.A.; Poklonski, N.A.; Lapchuk, N.M.; Khomich, A.A.; Dravin, V.A.; Poklonskaya, O.N.; Ashkinazi, E.E.; Vlasov, I.I.; Zavedeev, E.V.; et al. Optical and paramagnetic properties of polycrystalline CVD-diamonds implanted with deuterium ions. *J. Appl. Spectrosc.* **2012**, *79*, 600–609. [[CrossRef](#)]
22. Remes, Z.; Sun, S.-J.; Varga, M.; Chou, H.; Hsu, H.-S.; Kromka, A.; Horak, P. Ferromagnetism appears in nitrogen implanted nanocrystalline diamond films. *J. Magn. Magn. Mater.* **2015**, *394*, 477–480. [[CrossRef](#)]
23. Talapatra, S.; Ganesan, P.G.; Kim, T.; Vajtai, R.; Huang, M.; Shima, M.; Ramanath, G.; Srivastava, D.; Deevi, S.C.; Ajayan, P.M. Irradiation-Induced Magnetism in Carbon Nanostructures. *Phys. Rev. Lett.* **2005**, *95*, 097201. [[CrossRef](#)] [[PubMed](#)]
24. Narayan, J.; Bhaumik, A. Novel phase of carbon, ferromagnetism, and conversion into diamond. *J. Appl. Phys.* **2015**, *118*, 215303. [[CrossRef](#)]
25. Bhaumik, A.; Nori, S.; Sachan, R.; Gupta, S.; Kumar, D.; Majumdar, A.K.; Narayan, J. Room-Temperature Ferromagnetism and Extraordinary Hall Effect in Nanostructured Q-Carbon: Implications for Potential Spintronic Devices. *ACS Appl. Nano Mater.* **2018**, *1*, 807–819. [[CrossRef](#)]
26. Yoshinaka, H.; Inubushi, S.; Wakita, T.; Yokoya, T.; Muraoka, Y. Formation of Q-carbon by adjusting sp^3 content in diamond-like carbon films and laser energy density of pulsed laser annealing. *Carbon* **2020**, *167*, 504–511. [[CrossRef](#)]
27. Thakur, B.; Reddy, S.S.; Deshpande, U.P.; Amarendra, G.; Chakravarty, S. Evidence of magnetism in RF magnetron sputtered deposited carbon films and investigation of its origin. *Carbon* **2019**, *154*, 485–496. [[CrossRef](#)]
28. Sharoyan, E.; Mirzakhanyan, A.; Gyulasaryan, H.; Sanchez, C.; Kocharian, A.; Bernal, O.; Manukyan, A. Ferromagnetism of Nanographite Structures in Carbon Microspheres. *IEEE Trans. Magn.* **2016**, *52*, 2300803. [[CrossRef](#)]
29. Rawat, P.S.; Srivastava, R.; Dixit, G.; Asokan, K. Structural, functional and magnetic ordering modifications in graphene oxide and graphite by 100 MeV gold ion irradiation. *Vacuum* **2020**, *182*, 109700. [[CrossRef](#)]
30. Li, L.-J.; Yang, X.-M.; Xia, H.-H.; He, Z.-T.; Zhou, X.-T.; Liu, X.-D. The Magnetic Order in Ion Irradiated Graphite. *Chin. Phys. Lett.* **2016**, *33*, 046101. [[CrossRef](#)]
31. Sharma, S.; Rostas, A.M.; Bordonali, L.; MacKinnon, N.; Weber, S.; Korvink, J.G. Micro and nano patternable magnetic carbon. *J. Appl. Phys.* **2016**, *120*, 235107. [[CrossRef](#)]
32. Liu, J.; Bi, H.; Morais, P.C.; Zhang, X.; Zhang, F.; Hu, L. Room-temperature Magnetism in Carbon Dots and Enhanced Ferromagnetism in Carbon Dots-Polyaniline Nanocomposite. *Sci. Rep.* **2017**, *7*, 2165. [[CrossRef](#)] [[PubMed](#)]
33. Setzer, A.; Esquinazi, P.D.; Buga, S.; Georgieva, M.T.; Reinert, T.; Venus, T.; Estrela-Lopis, I.; Ivashenko, A.; Bondarenko, M.; Böhlmann, W.; et al. Nanometers-Thick Ferromagnetic Surface Produced by Laser Cutting of Diamond. *Materials* **2022**, *15*, 1014. [[CrossRef](#)] [[PubMed](#)]
34. Kononenko, V.V.; Khomich, A.A.; Khomich, A.V.; Khmel'nitskii, R.A.; Gololobov, V.M.; Komlenok, M.S.; Orekhov, A.S.; Orekhov, A.S.; Konov, V.I. Highly oriented graphite produced by femtosecond laser on diamond. *Appl. Phys. Lett.* **2019**, *114*, 251903. [[CrossRef](#)]
35. Khomich, A.A.; Kononenko, V.; Kudryavtsev, O.; Zavedeev, E.; Khomich, A.V. Raman Study of the Diamond to Graphite Transition Induced by the Single Femtosecond Laser Pulse on the (111) Face. *Nanomaterials* **2022**, *13*, 162. [[CrossRef](#)] [[PubMed](#)]
36. Webb, J.L.; Clement, J.D.; Troise, L.; Ahmadi, S.; Johansen, G.J.; Huck, A.; Andersen, U.L. Nanotesla sensitivity magnetic field sensing using a compact diamond nitrogen-vacancy magnetometer. *Appl. Phys. Lett.* **2019**, *114*, 231103. [[CrossRef](#)]
37. Xu, Y.; Zhang, W.; Tian, C. Recent advances on applications of NV⁻ magnetometry in condensed matter physics. *Photonics Res.* **2023**, *11*, 393–412. [[CrossRef](#)]
38. Zhang, Z.-D.; Yin, S.-Y.; Wang, L.-C.; Wang, Y.-D.; Li, Y.-F.; Tian, Z.-N.; Chen, Q.-D. Single NV centers array preparation and static magnetic field detection. *Opt. Express* **2022**, *30*, 32355–32365. [[CrossRef](#)]
39. Fujiwara, M.; Inoue, S.; Masuno, S.-I.; Fu, H.; Tokita, S.; Hashida, M.; Mizuochi, N. Creation of NV centers over a millimeter-sized region by intense single-shot ultrashort laser irradiation. *APL Photon.* **2023**, *8*, 036108. [[CrossRef](#)]
40. Pimenov, S.M.; Khomich, A.A.; Neuenschwander, B.; Jäggi, B.; Romano, V. Picosecond-laser bulk modification induced enhancement of nitrogen-vacancy luminescence in diamond. *J. Opt. Soc. Am. B* **2016**, *33*, B49–B55. [[CrossRef](#)]
41. Khveshchenko, D.V. Magnetic-Field-Induced Insulating Behavior in Highly Oriented Pyrolytic Graphite. *Phys. Rev. Lett.* **2001**, *87*, 206401. [[CrossRef](#)] [[PubMed](#)]
42. Park, N.; Yoon, M.; Berber, S.; Ihm, J.; Osawa, E.; Tománek, D. Magnetism in All-Carbon Nanostructures with Negative Gaussian Curvature. *Phys. Rev. Lett.* **2003**, *91*, 237204. [[CrossRef](#)] [[PubMed](#)]
43. Lehtinen, P.O.; Foster, A.S.; Ma, Y.; Krasheninnikov, A.V.; Nieminen, R.M. Irradiation-Induced Magnetism in Graphite: A Density Functional Study. *Phys. Rev. Lett.* **2004**, *93*, 187202. [[CrossRef](#)]
44. Hadipour, H. Screening of Coulomb interaction and π magnetism in defected graphene. *Phys. Rev. B* **2019**, *99*, 075102. [[CrossRef](#)]
45. Červenka, J.; Katsnelson, M.I.; Flipse, C.F.J. Room-temperature ferromagnetism in graphite driven by two-dimensional networks of point defects. *Nat. Phys.* **2009**, *5*, 840–844. [[CrossRef](#)]
46. Ugeda, M.M.; Brihuega, I.; Guinea, F.; Gómez-Rodríguez, J.M. Missing Atom as a Source of Carbon Magnetism. *Phys. Rev. Lett.* **2010**, *104*, 096804. [[CrossRef](#)]
47. Thakur, B.; Chandra Shekar, N.V.; Chandra, S.; Chakravarty, S. Effect of sp hybridization and bond-length disorder on magnetism in amorphous carbon—A first-principles study. *Diam. Relat. Mater.* **2022**, *121*, 108725. [[CrossRef](#)]
48. Karkin, A.E.; Voronin, V.I.; Berger, I.F.; Kazantsev, V.A.; Ponomov, Y.S.; Ralchenko, V.G.; Konov, V.I.; Goshchitskii, B.N. Neutron irradiation effects in chemical-vapor-deposited diamond. *Phys. Rev. B* **2008**, *78*, 033204. [[CrossRef](#)]

49. Khomich, A.A.; Khmel'nitskiy, R.A.; Khomich, A.V. Probing the Nanostructure of Neutron-Irradiated Diamond Using Raman Spectroscopy. *Nanomaterials* **2019**, *10*, 1166. [CrossRef]
50. Poklonskaya, O.N. Electron spin resonance of CVD diamonds irradiated with neutrons: State of spin glass. *BSU Bull. Phys. Math. Inform.* **2013**, *2*, 60–65. Available online: <http://elib.bsu.by/handle/123456789/95908> (accessed on 15 May 2023). (In Russian)
51. Garcia, M.A.; Fernandez Pinel, E.; de la Venta, J.; Quesada, A.; Bouzas, V.; Fernández, J.F.; Romero, J.J.; Martín González, M.S.; Costa-Krämer, J.C. Sources of experimental errors in the observation of nanoscale magnetism. *J. Appl. Phys.* **2009**, *105*, 013925. [CrossRef]
52. Nikolaenko, V.A.; Gordeev, V.G. Diamond amorphization in neutron irradiation. *Radiat. Eff. Defects. Solids* **1996**, *139*, 183–188. [CrossRef]
53. Esquinazi, P.D. (Ed.) *Basic Physics of Functionalized Graphite*; Springer: Cham, Switzerland, 2016. [CrossRef]
54. Orwa, J.O.; Nugent, K.W.; Jamieson, D.N.; Prawer, S. Raman investigation of damage caused by deep ion implantation in diamond. *Phys. Rev. B* **2000**, *62*, 5461–5472. [CrossRef]
55. Khomich, A.A.; Averin, A.A.; Poklonskaya, O.N.; Bokova-Sirosh, S.N.; Dzeraviah, A.N.; Khmel'nitskiy, R.A.; Vlasov, I.I.; Shenderova, O.; Poklonski, N.A.; Khomich, A.V. Features of the 1640 cm^{-1} band in the Raman spectra of radiation-damaged and nano-sized diamonds. *J. Phys. Conf. Ser.* **2019**, *1400*, 044017. [CrossRef]
56. Zaitsev, A.M. *Optical Properties of Diamond. A Data Handbook*; Springer: Berlin, Germany, 2001. [CrossRef]
57. Klein, C.A.; Hartnett, T.M.; Robinson, C.J. Critical-point phonon frequencies of diamond. *Phys. Rev. B* **1992**, *45*, 12854–12863. [CrossRef] [PubMed]
58. Nazaré, M.H.; Neves, A.J. (Eds.) *Properties, Growth and Applications of Diamond*; INPEC, IEE: London, UK, 2001.
59. Bosak, A.; Krisch, M. Phonon density of states probed by inelastic x-ray scattering. *Phys. Rev. B* **2005**, *72*, 224305. [CrossRef]
60. Richter, H.; Wang, Z.P.; Ley, L. The one phonon Raman spectrum in microcrystalline silicon. *Solid State Commun.* **1981**, *39*, 625–629. [CrossRef]
61. Osswald, S.; Mochalin, V.N.; Havel, M.; Yushin, G.; Gogotsi, Y. Phonon confinement effects in the Raman spectrum of nanodiamond. *Phys. Rev. B* **2009**, *80*, 075419. [CrossRef]
62. Khmel'nitskiy, R.A.; Dravin, V.A.; Tal, A.A.; Latushko, M.I.; Khomich, A.A.; Khomich, A.V.; Trushin, A.S.; Alekseev, A.A.; Terentiev, S.A. Mechanical stresses and amorphization of ion-implanted diamond. *Nucl. Instr. Meth. Phys. Res. B* **2013**, *304*, 5–10. [CrossRef]
63. Prawer, S.; Nugent, K.W.; Jamieson, D.N.; Orwa, J.O.; Bursill, L.A.; Peng, J.L. The Raman spectrum of nanocrystalline diamond. *Chem. Phys. Lett.* **2000**, *332*, 93–97. [CrossRef]
64. Chumakov, A.I.; Monaco, G.; Han, X.; Xi, L.; Bosak, A.; Paolasini, L.; Chernyshov, D.; Dyadkin, V. Relation between the boson peak in glasses and van Hove singularity in crystals. *Philos. Mag.* **2016**, *96*, 743–753. [CrossRef]
65. Nemanich, R.J. Low-frequency inelastic light scattering from chalcogenide glasses and alloys. *Phys. Rev. B* **1997**, *16*, 1655–1674. [CrossRef]
66. Khomich, A.V.; Khmel'nitskiy, R.A.; Hu, X.J.; Khomich, A.A.; Popovich, A.F.; Vlasov, I.I.; Dravin, V.A.; Chen, Y.G.; Karkin, A.E.; Ralchenko, V.G. Radiation Damage Effects on Optical, Electrical, and Thermophysical Properties of CVD Diamond Films. *J. Appl. Spectrosc.* **2013**, *80*, 707–714. [CrossRef]
67. Poklonskaya, O.N.; Vyrko, S.A.; Khomich, A.A.; Averin, A.A.; Khmel'nitskiy, R.A.; Poklonski, N.A. Raman Scattering in Natural Diamond Crystals Implanted with High-Energy Ions and Irradiated with Fast Neutrons. *J. Appl. Spectrosc.* **2014**, *81*, 969–977. [CrossRef]
68. Poklonskaya, O.N.; Khomich, A.A. Raman Scattering in a Diamond Crystal Implanted by High-Energy Nickel Ions. *J. Appl. Spectrosc.* **2013**, *80*, 715–720. [CrossRef]
69. Casari, C.S.; Bassi, A.L.; Baserga, A.; Ravagnan, L.; Piseri, P.; Lenardi, C.; Tommasini, M.; Milani, A.; Fazzi, D.; Bottani, C.E.; et al. Low-frequency modes in the Raman spectrum of $sp-sp^2$ nanostructured carbon. *Phys. Rev. B* **2008**, *77*, 195444. [CrossRef]
70. Ferrari, A.C.; Robertson, J. Interpretation of Raman spectra of disordered and amorphous carbon. *Phys. Rev. B* **2000**, *61*, 14095–14107. [CrossRef]
71. Kalish, R.; Reznik, A.; Prawer, S.; Saada, D.; Adler, J. Ion-implantation-induced defects in diamond and their annealing: Experiment and simulation. *Phys. Status Solidi A* **1999**, *174*, 83–99. [CrossRef]
72. Ziegler, J.F.; Ziegler, M.D.; Biersack, J.P. SRIM—The stopping and range of ions in matter (2010). *Nucl. Instr. Meth. Phys. Res. B* **2013**, *268*, 1818–1823. [CrossRef]
73. Khmel'nitskiy, R.A.; Dravin, V.A.; Tal, A.A.; Zavedeev, E.V.; Khomich, A.A.; Khomich, A.V.; Alekseev, A.A.; Terentiev, S.A. Damage accumulation in diamond during ion implantation. *J. Mater. Res.* **2015**, *30*, 1583–1592. [CrossRef]
74. Nikolaenko, V.A.; Krasikov, E.A. Effect of Reactor Radiation Intensity on Crystal Lattice Expansion in Diamond. *At. Energy* **2014**, *115*, 267–276. [CrossRef]
75. Ziegler, J.F.; Biersack, J.P.; Ziegler, M.D. *SRIM—The Stopping and Range of Ions in Matter*; SRIM Co.: Chester, MD, USA, 2008; Available online: <http://www.srim.org> (accessed on 15 May 2023).
76. Prins, J.F. Ballistic self-annealing during ion implantation. *J. Phys. D Appl. Phys.* **2001**, *34*, 3003–3010. [CrossRef]
77. Khomich, A.V.; Khmel'nitskiy, R.A.; Dravin, V.A.; Gippius, A.A.; Zavedeev, E.V.; Vlasov, I.I. Radiation damage in diamonds subjected to helium implantation. *Phys. Solid State* **2007**, *49*, 1661–1665. [CrossRef]
78. Hickey, D.P.; Jones, K.S.; Elliman, R.G. Amorphization and graphitization of single-crystal diamond—A transmission electron microscopy study. *Diam. Relat. Mater.* **2009**, *18*, 1353–1359. [CrossRef]

79. Bokobza, L.; Bruneel, J.-L.; Couzi, M. Raman Spectra of Carbon-Based Materials (from Graphite to Carbon Black) and of Some Silicone Composites. *C J. Carbon Res.* **2015**, *1*, 77–94. [CrossRef]
80. Ferrari, A.C.; Meyer, J.C.; Scardaci, V.; Casiraghi, C.; Lazzeri, M.; Mauri, F.; Piscanec, S.; Jiang, D.; Novoselov, K.S.; Roth, S.; et al. Raman spectrum of graphene and graphene layers. *Phys. Rev. Lett.* **2006**, *97*, 187401. [CrossRef]
81. Ferrari, A.C.; Basko, D.M. Raman spectroscopy as a versatile tool for studying the properties of graphene. *Nat. Nanotechnol.* **2013**, *8*, 235–246. [CrossRef]
82. Jorio, A. Raman Spectroscopy in Graphene-Based Systems: Prototypes for Nanoscience and Nanometrology. *Int. Sch. Res. Netw.* **2012**, *2012*, 234216. [CrossRef]
83. Davydov, S.Y.; Tikhonov, S.K. Magnetic susceptibility of wide-gap semiconductors. *Semiconductors* **1996**, *30*, 375–376.
84. Garg, A. The two cultures: SI and Gaussian units in electromagnetism. *Eur. J. Phys.* **2018**, *39*, 045205. [CrossRef]
85. Goldfarb, R.B. Electromagnetic Units, the Giorgi System, and the Revised International System of Units. *IEEE Magn. Lett.* **2018**, *9*, 1205905. [CrossRef] [PubMed]
86. Novikov, N.V. (Ed.) *Physical Properties of Diamond. Handbook*; Naukova Dumka: Kiev, Ukraine, 1987. (In Russian)
87. Madelung, O. *Semiconductors: Data Handbook*; Springer: Berlin, Germany, 2004. [CrossRef]
88. Poklonski, N.A.; Lapchuk, T.M.; Gorbachuk, N.I.; Nikolaenko, V.A.; Bachuchin, I.V. Nanostructuring of crystalline grains of natural diamond using ionizing radiation. *Semiconductors* **2005**, *39*, 894–897. [CrossRef]
89. Poklonski, N.A.; Dzeraviah, A.N.; Vyrko, S.A.; Zabrodskii, A.G.; Veinger, A.I.; Semenikhin, P.V. Curie–Weiss behavior of the low-temperature paramagnetic susceptibility of semiconductors doped and compensated with hydrogen-like impurities. *AIP Adv.* **2021**, *11*, 055016. [CrossRef]
90. Lavrik, N.L.; Voloshin, V.P. Calculation of mean distances between the randomly distributed particles in the model of points and hard spheres (the method of Voronoi polyhedra). *J. Chem. Phys.* **2001**, *114*, 9489–9491. [CrossRef]
91. Khomich, A.A.; Dzeraviah, A.N.; Poklonskaya, O.N.; Khomich, A.V.; Khmelnskiy, R.A.; Poklonski, N.A.; Ralchenko, V.G. Effect of neutron irradiation on the hydrogen state in CVD diamond films. *J. Phys. Conf. Ser.* **2018**, *1135*, 012019. [CrossRef]
92. Zabrodskii, A.G. Magnetic ordering in doped semiconductors near the metal–insulator transition. *Phys. Status Solidi B* **2004**, *241*, 33–39. [CrossRef]
93. Lebedev, A.A.; Abramov, P.L.; Agrinskaya, N.V.; Kozub, V.I.; Lebedev, S.P.; Oganessian, G.A.; Tregubova, A.S.; Shamshur, D.V.; Skvortsova, M.O. Metal-insulator transition in *n*-3C-SiC epitaxial films. *J. Appl. Phys.* **2009**, *105*, 023706. [CrossRef]
94. Kavaleu, A.I.; Gorbachuk, N.I.; Vyrko, S.A.; Poklonski, N.A.; Kozlova, M.V.; Dravin, V.A.; Khomich, A.V. Optical and electrical properties of crystalline natural and polycrystalline CVD diamonds irradiated with fast reactor neutrons. In *Interaction of Radiation with Solids (IRS-2019), Proceedings of the 13th International Conference, Minsk, Belarus, 30 September–3 October 2019*; BSU: Minsk, Belarus, 2019; pp. 265–268. Available online: <http://elib.bsu.by/handle/123456789/241542> (accessed on 15 May 2023). (In Russian)
95. Zhou, S. Defect-induced ferromagnetism in semiconductors: A controllable approach by particle irradiation. *Nucl. Instr. Meth. Phys. Res. B* **2014**, *326*, 55–60. [CrossRef]
96. Botsch, L.; Esquinazi, P.D.; Bundesmann, C.; Spemann, D. Toward a systematic discovery of artificial functional magnetic materials. *Phys. Rev. B* **2021**, *104*, 014428. [CrossRef]
97. Mal, S.; Nori, S.; Jin, C.; Narayan, J.; Nellutla, S.; Smirnov, A.I.; Prater, J.T. Reversible room temperature ferromagnetism in undoped zinc oxide: Correlation between defects and physical properties. *J. Appl. Phys.* **2010**, *108*, 073510. [CrossRef]
98. Khomich, A.A.; Kovalev, A.I.; Khmelnskiy, R.A.; Khomich, A.V.; Popovich, A.F.; Ralchenko, V.G. Engineering of defects in fast neutron irradiated synthetic diamonds. *J. Phys. Conf. Ser.* **2021**, *2103*, 012076. [CrossRef]
99. Massi, L.; Fritsch, E.; Collins, A.T.; Hainschwang, T.; Notari, F. The “amber centres” and their relation to the brown colour in diamond. *Diam. Relat. Mater.* **2005**, *14*, 1623–1629. [CrossRef]
100. Hainschwang, T.; Notari, F.; Pamies, G. A Defect Study and Classification of Brown Diamonds with Deformation-Related Color. *Minerals* **2020**, *10*, 903. [CrossRef]
101. Mäki, J.-M.; Tuomisto, F.; Kelly, C.J.; Fisher, D.; Martineau, P.M. Properties of optically active vacancy clusters in type IIa diamond. *J. Phys. Condens. Matter* **2009**, *21*, 364216. [CrossRef]
102. Hounsborne, L.S.; Jones, R.; Martineau, P.M.; Fisher, D.; Shaw, M.J.; Briddon, P.R.; Öberg, S. Origin of brown coloration in diamond. *Phys. Rev. B* **2006**, *73*, 125203. [CrossRef]
103. Stauffer, D.; Aharony, A. *Introduction to Percolation Theory*; Taylor & Francis: London, UK, 1994. [CrossRef]

Disclaimer/Publisher’s Note: The statements, opinions and data contained in all publications are solely those of the individual author(s) and contributor(s) and not of MDPI and/or the editor(s). MDPI and/or the editor(s) disclaim responsibility for any injury to people or property resulting from any ideas, methods, instructions or products referred to in the content.